Resistive switching in metallic Ag2S memristors due to a local overheating induced phase transition

Journal Article

Author(s):
Gubicza, Agnes; Csontos, Miklos; Halbritter, András; Mihály, György

Publication date:
2015-07-14

Permanent link:
https://doi.org/10.3929/ethz-b-000581368

Originally published in:
Nanoscale 7(26), https://doi.org/10.1039/c5nr02536b

Nanoscale

COMMUNICATION

Cite this: *Nanoscale*, 2015, **7**, 11248

Received 19th April 2015,
Accepted 25th May 2015

DOI: 10.1039/c5nr02536b

www.rsc.org/nanoscale

Resistive switching in metallic Ag_2S memristors due to a local overheating induced phase transition

Agnes Gubicza,[a,b] Miklós Csontos,*[a] András Halbritter[a,b] and György Mihály[a,b]

Resistive switchings in nanometer-scale metallic junctions formed between an inert metallic tip and an Ag film covered by a thin Ag_2S layer are investigated as a function of temperature at different biasing conditions. The observed switching threshold voltages along with the ON and OFF state resistances are quantitatively understood by taking the local overheating of the junction volume and the resulting structural phase transition of the Ag_2S matrix into account. Our results demonstrate that the essential characteristics of the resistive switching in Ag_2S based nanojunctions can be routinely optimized by suitable sample preparation and biasing schemes.

Self-assembled nanostructures with tunable electrical properties have been intensively studied as potential candidates to replace the present day CMOS devices. Conducting nanofilaments formed by reversible solid state electrochemical reactions between metallic electrodes have been demonstrated to be suitable for logical and non-volatile resistance switching random access memory (ReRAM)[1–15] operations at dimensions which are inaccessible in present day's silicon based technology.[16] The resistance of such a two-terminal device, called memristor,[17] is modified at higher bias voltages ($V > V_{th}$), while readout is performed at $V \ll V_{th}$ without altering the stored information.

Oxidation, activated ionic transport and reduction were identified as the leading mechanisms of nanofilament formation and rupture in solid state electrolytes[4,7,15,18–35] giving rise to resistive changes in the tunneling regime between insulating $R_{OFF} \gg 10$ MΩ and $R_{ON} \approx h/2e^2 = 12.9$ kΩ resistance values, the latter is often considered as the hallmark of atomic sized contacts. Such devices, however, could only be operated at reduced switching speeds due to their fundamental RC limitations. Intensive studies of the metallic regime with electrical conduction taking place *via* 10–15 nm wide filaments were started recently in metal oxide based memristive systems where a Joule heating assisted activated ion and/or oxygen vacancy migration have been found to play a key role in the observed resistive switchings.[36–38]

Our previous experiments[39,40] based on the ionic conductor Ag_2S have demonstrated reproducible, nanosecond timescale resistive switchings and robustness against low voltage read-out operations at room temperature exhibiting R_{OFF}/R_{ON} ratios of 2–10. Resistive switching is attributed to metallic conduction channels with changing diameter in the range of 2–5 nm while they are exposed to current densities as high as 10^{10} A cm^{-2}.

Here we report on extensive measurements and a thorough statistical analysis performed in order to explore the effect of the environment's temperature, the series resistance of the biasing circuit and the amplitude of the biasing signal on the technologically most relevant parameters, the ON and OFF switching threshold voltages, R_{ON} and R_{OFF}. We discuss the role of a highly non-equilibrium mechanism characteristic to the metallic regime. We demonstrate that our data are in quantitative agreement with a model taking pronounced power dissipation released at the nanojunction's length scale into account, giving rise to a local overheating of the junction up to the superionic phase transition of the Ag_2S layer even at cryogenic ambient temperatures. This accelerates the field driven, thermally activated ionic migration processes as well as electrode reactions. The observed resistive switchings are attributed to an enhanced filament reconfiguration accompanying the structural phase transition of the Ag_2S matrix.

During sample fabrication an 80 nm thick Ag layer was deposited onto a Si substrate followed by a 5-minute long sulfurisation resulting in a 30 nm thick stoichiometric Ag_2S layer on top of the Ag electrode.[41] Nanometer-scale junctions were created between the Ag_2S surface and a mechanically sharpened PtIr tip in STM geometry. The V_{drive} triangular voltage output of a low output impedance data acquisition card was acting on the memristive junction and on a variable series resistor R_S as shown in the inset of Fig. 1(b). The device's current was monitored by a current amplifier operating at a

[a]Department of Physics, Budapest University of Technology and Economics, Budafoki ut 8, 1111 Budapest, Hungary. E-mail: csontos@dept.phy.bme.hu
[b]MTA-BME Condensed Matter Research Group, Budafoki ut 8, 1111 Budapest, Hungary

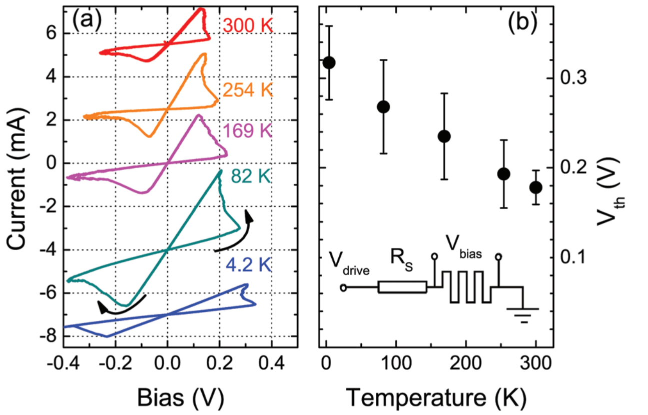

Fig. 1 (a) Representative *I–V* traces of metallic PtIr–Ag_2S–Ag junctions recorded at various temperatures from T = 4.2 K to room temperature. The direction of the loops indicated by the arrows was identical for all curves. The traces are vertically shifted for clarity. (b) The OFF to ON switching threshold voltage V_{th} as a function of temperature. The dots and the error bars correspond to the average and standard deviation as evaluated for ~10^3 traces at each temperature, respectively. The inset shows the electrical circuit diagram of the biasing setup.

typical gain of 10^4. The V_{bias} voltage drop on the junction was determined numerically as $V_{bias} = V_{drive} - I{\cdot}R_S$ where the 50 Ω input impedance of the current amplifier was also accounted for in R_S. By convention, a positive bias corresponds to a positive voltage applied to the Ag layer with respect to the PtIr electrode. The measurements were performed in the variable temperature insert of a standard ^{4}He cryostat between 4.2 K and room temperature. Approximately 10^3 stable current–voltage (*I–V*) traces were acquired at each temperature at various R_S values ranging from 50 to 400 Ω.

Typical *I–V* traces recorded within 300 ms (corresponding to a typical, low bias sweep rate of 5–10 V s^{-1}) at selected temperatures are illustrated in Fig. 1(a). At low bias voltages the initial OFF state resistance R_{OFF} is measured. Increasing V_{bias} to a temperature dependent switching threshold V_{th} = 180–320 mV a reconfiguration takes place resulting in a drop of the junction's resistance from $R_{OFF} \approx 10^3$ Ω to $R_{ON} \approx 10^2$ Ω. Decreasing V_{bias} preserves R_{ON} until a negative threshold of 80–250 mV is reached where the onset of the transition from the ON to the initial OFF state occurs. The direction of the resulting hysteresis loops was identical for all curves and is indicated by the arrows in Fig. 1(a). The monotonic decrease in V_{th} with increasing temperature is emphasized by the statistical analysis of the ~10^4 stable *I–V* traces (approximately 2000 at each temperature) as shown in Fig. 1(b).

The influence of R_S on R_{ON} and R_{OFF} is shown in Fig. 2(a) and (b), respectively. The initial OFF state resistances are determined to a great extent by the controlled approach procedure of the STM tip and thus are not expected to exhibit any dependence on the biasing scheme. Consequently, a systematic R_S dependence of R_{OFF} was not observed, either, as demonstrated by the uniformly scattered red dots in Fig. 2(b). On the other hand, R_{ON} is seen to be proportional to R_S as indicated by the

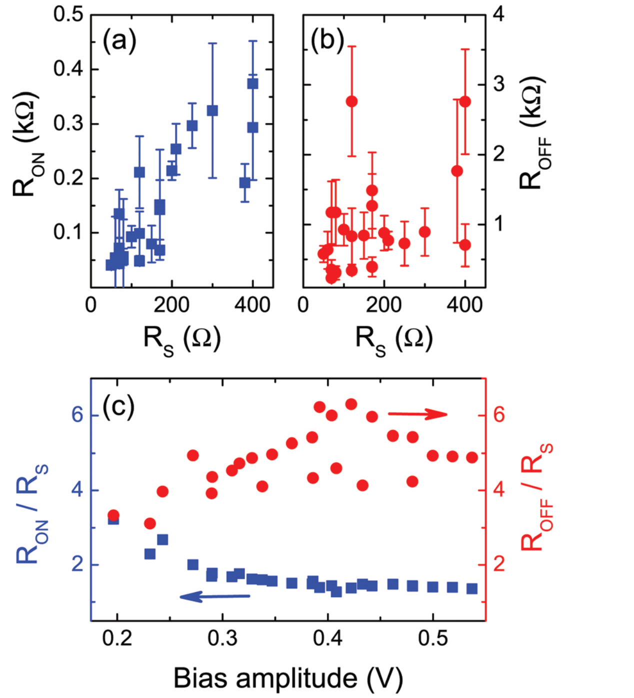

Fig. 2 Average and standard deviation of the ON (a) and OFF (b) state resistances R_{ON} and R_{OFF} acquired at various temperatures at 4.2 K < T < 300 K and at V^0_{drive} = 0.6 V as a function of the series resistance R_S. Note the different scales on (a) and (b). (c) R_{ON}/R_S (blue squares) and R_{OFF}/R_S (red dots) as a function of the bias voltage amplitude measured in a single junction at T = 300 K and R_S = 50 Ω.

blue squares in Fig. 2(a). The latter behavior is attributed to the decreasing voltage drop on the junction as its resistance is decreasing toward R_S upon an OFF to ON transition resulting in a rate limitation for a further resistance change as discussed in ref. 40. This is also in agreement with the observed dependence of R_{OFF} and R_{ON} on the bias voltage amplitude as displayed in Fig. 2(c) for a representative single junction measured at room temperature, *i.e.* R_{ON} saturates at the scale of R_S as the driving amplitude is increased.

Next we investigate the self-heating effect characteristic to nanometer-scale metallic junctions exposed to finite bias voltages and show that our data acquired over a broad temperature range from T = 4.2 K to room temperature are consistent with a phase change model exploiting extensive power dissipation released in the junction's volume.

Power dissipation in point contacts is concentrated in a small volume around the contact center, leading to an elevated temperature in the junction area.[42] Assuming that only electrons, subject to a diffusive motion, carry the heat and the L_i inelastic diffusion length exceeds the d contact diameter, *i.e.* $l_e < d < L_i$ with l_e being the elastic mean free path, the junction's local temperature is given by

$$T_J^{\,2} = T^2 + \frac{9e^2}{4\pi^3 k_B^2}\frac{d}{L_i}V_{bias}^{\;2}, \tag{1}$$

where T is the equilibrium temperature of the leads[43] as it was demonstrated experimentally in ferromagnetic contacts by the observation of a finite bias induced ferromagnetic phase transition.[44] A detailed derivation of eqn (1) along with the discussion of the so-called thermal ($d > L_i$) and ballistic ($d < l_e$) regimes are given in the Appendix. Inserting our typical junction diameters[39] of 2–5 nm, L_i ~10 nm and the observed switching threshold of a few 100 mV into eqn (1) reveals that the $T_J = T_C = 451$ K bulk structural phase transition temperature of Ag_2S is easily reached even at an ambient temperature of $T = 4.2$ K. While the low temperature acanthite phase of Ag_2S is a semiconductor with very low conductivity, its high temperature argentite phase is a superionic conductor exhibiting a highly enhanced ionic mobility.[45] It has also been demonstrated[8,22] that the bulk T_C is considerably reduced in the presence of an applied electric field facilitating the initial growth of the metallic Ag nanofilaments in high OFF state resistance devices. The detailed microscopic picture of the electric field driven ionic motion is a subject of on-going molecular dynamical simulations. However, the above numerical estimation implies that a Joule heating assisted local superionic phase transition of the Ag_2S solid electrolyte may play a major role in the observed resistive switchings. Based on a recent study on the dynamics of nanoscale metallic inclusions in dielectrics[35] we anticipate a continuous, bulk filament growth in our Ag_2S system characterized by high oxidation and reduction rates as well as by a high ion mobility.[1] It is to be added that another relevant, highly non-equilibrium contributions, *e.g.* surface atom diffusion and electron wind forces, may also arise from the strong, inhomogeneous electric field and high current density, respectively.

Based on the above considerations we interpret the observed switching cycle along with the schematic illustrations displayed in Fig. 3 as follows. We point out that in a steady state the junction's temperature is determined by the $P = I{\cdot}V_{bias}$ power dissipation resulting in the emergence of isothermal regions along the $I{\cdot}V_{bias}$ = constant lines in the I–V plane of the device as indicated by the dashed lines in Fig. 3(b). Note that the steady state is classified here by a time scale which is shorter than that of the resistance change at the actual bias voltage[40] but long enough for the establishment of a stable temperature profile around the contact volume. We emphasize that the $I{\cdot}V_{bias}$ = constant equation of the isothermal lines directly follows from eqn (1) by assuming an orifice-shaped, diffusive nanojunction where $G = 1/R = \sigma d$ with σ being the electrical conductivity[46] and thus $T_J^2 - T^2$ is proportional to $G{\cdot}V_{bias}^2 = I{\cdot}V_{bias}$. We believe that a narrowest cross-section dominating the electronic transport properties necessarily exists along the metallic filament and its shape can be well approximated by an orifice-like profile. However, a nanowire-like, uniformly elongated constriction of the length l can also be taken into account here. In the latter case $G = \sigma d^2/l$ applies, resulting in isothermal regions situated along the steeper, $I{\cdot}V_{bias}^3$ = constant lines. In reality, these two scenarios can be considered as limiting cases for the isothermal lines corresponding to arbitrary filament geometries. The exact form of these lines, however, does not play a role in our argumentation.

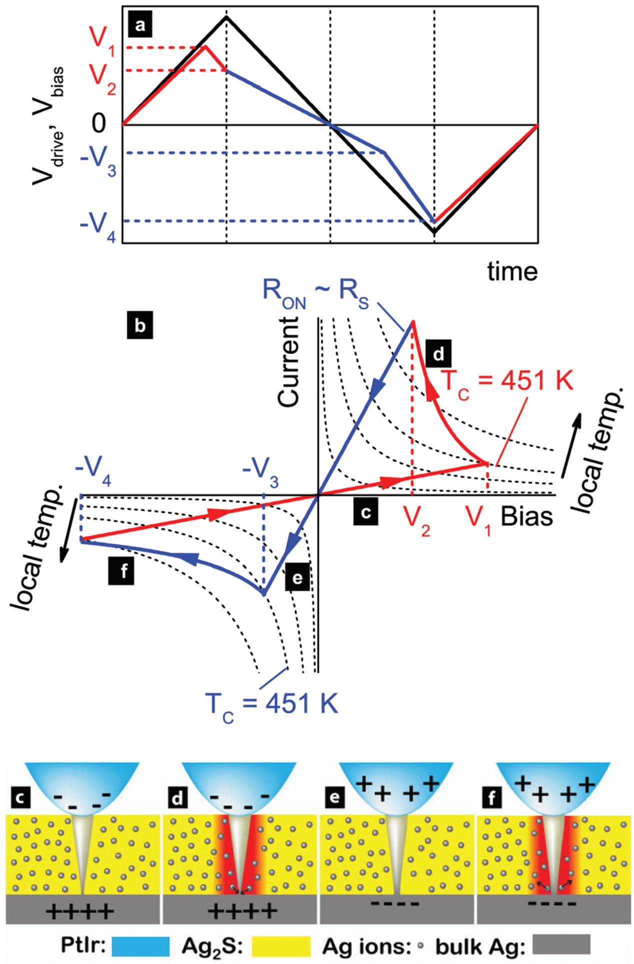

Fig. 3 (a) Schematic illustration of the recorded voltage signals. $V_{drive}(t)$ (black) is the triangular voltage acting on R_S and the junction. The V_{bias} voltage drop is indicated by red (blue) in the OFF (ON) state. The four V_{bias} values characterizing the resistive switching cycle are labeled accordingly. (b) Schematic illustration of the switching cycle at the I–V plane starting from the OFF state at zero bias in the framework of the thermally assisted phase change model. Along the dashed hyperbolae the $I{\cdot}V_{bias}$ dissipated power along with the T_J local temperature of the junction are constant. Electrical conductance *via* the metallic filament in the OFF (c) and ON (e) states as well as during the OFF to ON (d) and ON to OFF (f) transitions are labeled on the I–V characteristics. (d) & (f) An enhanced filament growth/shrinkage is expected to take place when the local temperature of the biased junction reaches the T_C = 451 K critical temperature of the superionic phase transition of the Ag_2S matrix in either field direction.

Compared to the predictions of eqn (1) the actual junction temperature may be reduced due to the fact that the filament is embedded in a semiconducting Ag_2S matrix exhibiting finite heat conduction. However, based on its poor electrical conductivity we do not expect a considerable cooling power on the junction mediated by the acanthite phase Ag_2S in our non-planar arrangement.

While ionic motions do occur within the filament volume also at $T_J < T_C$ leading to a slow reconfiguration of the conducting channel and thus to a small, systematic positive deviation from a linear *I–V* characteristics in the initial OFF state at a negatively charged inert electrode [Fig. 3(c)], the onset of an enhanced filament growth takes place when at $V_{bias} = V_1 = V_{th}$ the local temperature around the contact reaches T_C and the surrounding Ag_2S matrix enters its superionic phase [Fig. 3(d)]. Due to the rapid filament growth taking place in the superionic argentite surrounding in the presence of strong electric fields during the OFF to ON switching, V_{bias} can be decreasing while V_{drive} is still increasing. This is not only the consequence of the increasing fraction of V_{drive} dropping on the series resistance at higher current levels but is also in agreement with eqn (1), *i.e.* at larger d the $T_J \geq T_C$ condition can be fulfilled at lower V_{bias}. At decreasing V_{bias} during the transition the characteristic time scale of the resistance change is exponentially diverging as reported in ref. 40. Consequently, a "final" ON state resistance is never strictly reached. However, any further resistance change would require either an unreasonably long time or unreasonably high V_{drive}, as will be discussed below. Therefore the OFF to ON transition at a given voltage sweep rate is naturally terminated as the junction's resistance becomes comparable to R_S, in agreement with the data shown in Fig. 2(a).

At oppositely charged electrodes the direction of ionic motion is reversed and acts toward the (partial) destruction of the conducting filament [Fig. 3(e)]. In this field direction the $T_J = T_C$ condition is fulfilled at a lower, $V_3 < V_1$ bias in accordance with eqn (1) as $d_{ON} > d_{OFF}$. Independently from the relationship of V_1 and V_2, $V_3 < V_2$ also holds because both points on the linear *I–V* trace belong to the same ON state exhibiting an identical resistance while they are subjected to different driving voltages of $V_{drive}(2) > |V_{drive}(3)|$, as illustrated in Fig. 3(a) and (b). The $V_4 > V_1$ relationship relies on similar considerations. These arguments make it evident that the hysteresis loops are necessarily asymmetric in V_{bias} exhibiting a longer and smoother transition from the ON to the OFF state rather than *vice versa*, which is in full agreement with the representative traces shown in Fig. 1(a).

Another important consequence of the $V_3 < V_1$ condition is $T_J(2) > T_J(1)$, *i.e.* the resistive switching is not an isothermal process. This implies that during a decreasing positive bias further resistance change is expected to take place in the ON state as long as $T_J > T_C$. The competing time scales of this inherent resistance change and that of the driving signal are demonstrated in Fig. 4. A single device was identically biased to its OFF to ON transition within 2.5 ms by a triangular signal with an amplitude of $V^0_{drive} = 0.5$ V. This was followed by different voltage sweeps at rates of −200 V s^{-1} (blue trace) and −2.5 V s^{-1} (green trace). In the latter case the on-going resistance change at higher biases corresponding to $T_J > T_C$ resulted in a further, well visible decrease in R_{ON} and a rounded upper corner of the hysteresis loop. In contrast, the fast sweep rate in the former experiment outperformed the reduced rate of the resistance change and yielded to an apparent linear *I–V* trace

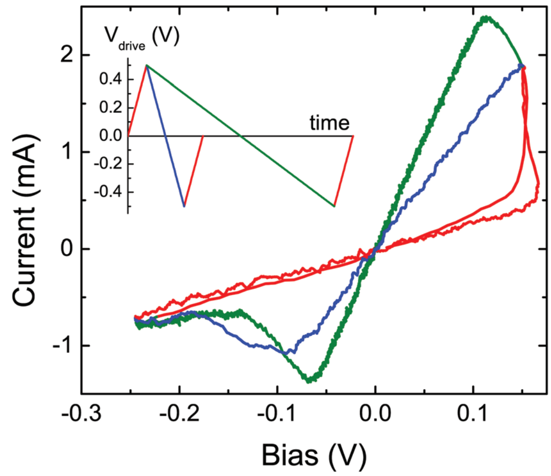

Fig. 4 *I–V* traces of a single junction recorded at different voltage sweep rates after the OFF to ON transition. The inset illustrates the different driving schemes with −200 V s^{-1} (blue) and −2.5 V s^{-1} (green) sweep rates. $V^0_{drive} = 0.5$ V, $R_{OFF} = 380\ \Omega$, $R_{ON} = 75\ \Omega$ (blue) and 45 Ω (green), $R_S = 50\ \Omega$.

and a sharp corner. The actual shape of the transition along with the achievable R_{OFF}/R_{ON} ratios are thus also largely determined by the frequency of the driving signal.[40]

At $V_{bias} = V_3$ the Ag_2S matrix becomes superionic again, fueling an accelerated filament destruction [Fig. 3(f)]. However, in contrast to the one responsible for the OFF to ON switching, this process is inherently self-limiting as at a decreasing d the magnitude of V_{bias} necessary to keep the $T_J = T_C$ condition satisfied is also increasing. Therefore, in order to achieve higher R_{OFF} values one has to supply an increased V_{bias}. The unambiguous identification of the terminating mechanism of the ON to OFF switching is not as straightforward as in the opposite case. However, the firm experimental finding that upon increasing the magnitude of the negative bias R_{OFF} always takes its initial value indicates that the Ag_2S matrix exposed to the strong electric field in the vicinity of the filament has a limited capability to incorporate the dissolved Ag^+ ions and this saturation concentration is close to the stoichiometric value which is present at the beginning of the switching cycle. It is also to be noted that in the Ag rich environment the argentite phase can survive even at room temperature.[22] Such residues may also contribute to the filament structure refining the simple picture of pure Ag channels depicted in Fig. 3(c)–(f).

The relevance of the above scenario is further supported by re-plotting the $V_1(T) = V_{th}(T)$ data of Fig. 1(b) along with the $V_3(T)$ ON to OFF switching threshold voltages against eqn (1) in a linearized fashion with $T_J = T_C = 451$ K, as shown in Fig. 5(a). While the thermal limit with $L_i/d = 1$ clearly remains unchallenged at the onset of the OFF to ON switching, even the low temperature enhancement in L_i, which presumably occurs due to suppressed phonon scattering, falls below an upper limit of $L_i/d = 6$. On the other hand, the ON to

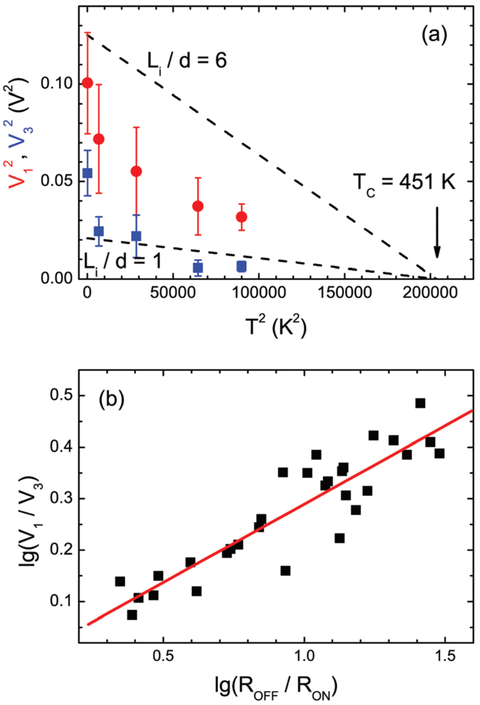

Fig. 5 (a) $V_1^2 = V_{th}^2$ (red dots) and V_3^2 (blue squares) as a function of T^2. The dots and the error bars correspond to the average and standard deviation as evaluated for ~10^3 traces at each temperature, respectively. The dashed lines are calculated by eqn (1) with $T_J = T_C = 451$ K and $L_i/d = 6$ (upper line) and 1 (lower line), the latter representing the thermal limit. (b) Logarithmic plot of V_1/V_3 *versus* R_{OFF}/R_{ON} with a linear fit to the data.

OFF switching takes place close to the thermal limit signalling that the relevant transport length scales, L_i, d and l_e fall close to each other within a few nanometers.

Fig. 5(b) shows the relationship of the ON and OFF switching threshold voltages to the corresponding R_{OFF} and R_{ON} values. As pointed out in the discussion of eqn (1), the requirement that the onsets of both transitions must occur as T_J approaches the same T_C sets the conditions of $(V_1/V_3)^2 = (R_{OFF}/R_{ON})^\alpha$ with $\alpha = 1$ and $\alpha = 1/2$ for the two limiting junction geometries of an orifice and a uniform nanowire, respectively. Arbitrary junction geometries are manifested in the intermediate values of α. The satisfactory linear fit to the corresponding logarithmic plot displaying data acquired at all investigated temperatures and R_S values reveals $\alpha = 0.61 \pm 0.06$ and thus provides a strong quantitative evidence to our picture.

In the intermediate regime situated on the verge of ballistic and diffusive conductance the d_{OFF} and d_{ON} average filament diameters are estimated based on the interpolating formula[47] based on the Boltzmann equation for arbitrary ratio of d/l_e

$$R = l_e/d\frac{16}{3\pi\sigma d} + \Gamma(l_e/d)\frac{1}{\sigma d}, \quad (2)$$

where $\Gamma(l_e/d)$ is a numerically determined monotonic function with $\Gamma(0) = 1$ and $\Gamma(\infty) = 0.694$. Note that the first term is exactly the Sharvin resistance by placing $\sigma = l_e^2 n/\hbar k_F$ Drude conductivity into the formula, thus it is actually independent of l_e. The junction diameters are calculated by taking $\lambda_F = 0.4$ nm, being the Fermi wavelength in bulk Ag, into account. This approximation results in the temperature independent values of $d_{OFF} = 1.8 \pm 0.7$ nm and $d_{ON} = 4.8 \pm 1.2$ nm confirming the range of validity of eqn (1), *i.e.* the $l_e \leq d < L_i$ assumption with $l_e = 1.8$ nm being the elastic mean free path in the argentite phase of Ag_2S.[48] These values are also in agreement with our recent study on the conducting channel distribution carried out by low temperature point contact Andreev reflection spectroscopy.[39]

In conclusion, we studied the resistive switching characteristics to metallic Ag_2S nanojunctions. We propose that the dominating driving force of the resistance change in the highly non-equilibrium metallic regime is self-heating assisted electric field driven ionic transport giving rise to an intensive expansion/shrinkage of the metallic conduction channel as the bias dependent local temperature of the nanojunction approaches the superionic phase transition temperature of the surrounding Ag_2S solid electrolyte. Based on the statistical analysis of ~10^4 *I–V* traces acquired at different biasing conditions over a wide temperature range we found that the technologically most relevant parameters, the ON and OFF switching threshold voltages as well as R_{ON} and R_{OFF} are determined by the controllable means of sample preparation, the series resistance of the biasing circuit and the ambient temperature, in quantitative agreement with the proposed model. In spite of the self-assembling nature of filament formation/destruction, our results demonstrate the merits of engineering and large scale production of nanometer-scale Ag_2S based memory cells exhibiting uniform behavior at technologically optimal device parameters.

Appendix

In this appendix power dissipation and local overheating in nanometer-scale junctions are discussed. In biased point contacts the major part of the potential drops within a characteristic distance of d from the contact center thus the power dissipation is also concentrated in a small volume resulting in elevated junction temperatures under an applied voltage. Assuming that the heat is conducted just by the electrons, the equations of heat conduction can be solved for an arbitrary point contact geometry.[49] These calculations are valid in the so-called thermal regime, where the d contact diameter is larger than the L_i inelastic diffusive length. In this limit the T_J temperature of the contact center is determined by the bias voltage as

$$T_J^2 = T^2 + \frac{V_{bias}^2}{4\mathcal{L}}, \quad (3)$$

where T is the temperature of the electrodes and $\mathcal{L} = (\pi k_B)^2/3e^2$ is the Lorentz number. The power is dissipated inside the junction within a characteristic volume of ~d^3. As the resistance of a diffusive contact is $R = 1/\sigma d$ with σ being the electrical conductivity,[46] the dissipated power scales with the contact diameter as $P = V_{\text{bias}}^2\sigma d$. According to eqn (3) these two factors give a contact temperature which is independent of d.

In smaller nanojunctions with $d < L_i$ the potential also drops within a distance of d from the contact center.[46] However, in this regime the electrons must travel a distance of L_i to dissipate the energy gained from the potential drop. Therefore the power $P = V^2\sigma d$ is dissipated in a volume of $\sim L_i^3$, regardless of the contact diameter. As the magnitude of power dissipation scales with d whereas its corresponding volume is constant, T_J is expected to decrease with decreasing contact size. These considerations can be quantified by the following calculation.

We consider an orifice-like contact and assume that the power dissipation takes place within a sphere with radius b around the contact whereas the $\mathcal{P}$ power density is constant in this volume. The continuity equation for the $\vec{j}_t$ thermal current density is given as

$$\oint_A \vec{j}_t \mathrm{d}\vec{A} = \int_V \mathcal{P} \mathrm{d}V. \tag{4}$$

The equation for the heat conduction is $\vec{j}_t = -\kappa\vec{\nabla}T$. If the heat is conducted solely by the electrons, the Wiedemann–Franz relation between the κ heat conductivity and the σ electrical conductivity is applied as $\kappa = \mathcal{L}T\cdot\sigma$ thus $\vec{j}_t$ can be written as $\vec{j}_t = -\mathcal{L}\sigma T\vec{\nabla}T = -(\mathcal{L}\sigma\vec{\nabla}T^2)/2$. Assuming that in the steady state the temperature depends only on the r distance from the contact center the continuity equation can be integrated as

$$2\pi r^2\mathcal{L}\sigma\frac{\mathrm{d}}{\mathrm{d}r}T^2 = -\frac{4}{3}\pi b^3\mathcal{P}, \quad \text{if} \quad r > b \tag{5}$$

$$2\pi r^2\mathcal{L}\sigma\frac{\mathrm{d}}{\mathrm{d}r}T^2 = -\frac{4}{3}\pi r^3\mathcal{P}, \quad \text{if} \quad r < b, \tag{6}$$

with the boundary condition of $T(r) \to T$ at $r \to \infty$.

In a voltage biased diffusive contact $\mathcal{P} = \left(V_b^2/R\right)/(4\pi b^3/3)$ and $R = 1/\sigma d$, so the temperature of the junction at $r = 0$ is

$$T_J^2 = T^2 + \frac{3}{4\pi}\frac{V_{\text{bias}}^2}{\mathcal{L}}\frac{d}{b}. \tag{7}$$

In the thermal regime the power is dissipated in a characteristic distance of d from the contact center, thus $b = d$ should be substituted into eqn (7) in agreement, apart from a small deviation in the numerical coefficient, with eqn (3).

As this simple calculation successfully reproduces the known results in the thermal limit, it can also be employed for smaller contacts with $d < L_i$. In this case $b = L_i$ is to be inserted into eqn (7) with the appropriate coefficient adopted from eqn (3) as

$$T_J^2 = T^2 + \frac{V_{\text{bias}}^2}{4\mathcal{L}}\frac{d}{L_i}. \tag{8}$$

Eqn (8) shows that T_J is reduced in smaller contacts and the magnitude of this reduction is determined by d/L_i.

In even smaller contacts with $d < l_e$ the electrons perform a ballistic motion and the resistance is determined by the Sharvin formula, $R = 16l_e/3\pi d^2\sigma$ thereby the temperature of the junction is written as

$$T_J^2 = T^2 + \frac{9}{64}\frac{V_b^2}{\mathcal{L}}\frac{d^2}{L_i l_e}. \tag{9}$$

It must be noted that the validity of these calculations in the $d < l_e$ regime is limited. As the electrons can only thermalize within a characteristic distance of L_i, the equations of heat conduction are not strictly applicable at shorter length scales. However, while the major part of the temperature increase takes place at a longer length-scale of $r > L_i$, the above formulae still provide a good estimation for the contact temperature within an error of ~33%. These calculations are also overestimating T_J when not only the distant electrodes are cooled but also the whole contact surface, for instance, in measurements performed under ambient conditions.

Acknowledgements

This work was supported by the Hungarian Research Funds OTKA K105735, K112918 and by the European Union 7th Framework Programme (Grant No. 293797). The technical assistance of A. Magyarkuti is acknowledged.

References

1 J. J. Yang, D. B. Strukov and D. R. Stewart, *Nat. Nanotechnol.*, 2013, **8**, 13–24.
2 J. Borghetti, G. S. Snider, P. J. Kuekes, J. J. Yang, D. R. Stewart and R. S. Williams, *Nature*, 2010, **464**, 873–876.
3 Y. V. Pershin and M. Di Ventra, *Phys. Rev. E: Stat. Phys., Plasmas, Fluids, Relat. Interdiscip. Top.*, 2011, **84**, 046703.
4 K. Terabe, T. Hasegawa, T. Nakayama and M. Aono, *Nature*, 2005, **433**, 47–50.
5 D. B. Strukov, G. S. Snider, D. R. Stewart and R. S. Williams, *Nature*, 2008, **453**, 80–83.
6 R. Waser and M. Aono, *Nat. Mater.*, 2007, **6**, 833–840.
7 K. Terabe, T. Hasegawa, C. Liang and M. Aono, *Adv. Mater.*, 2007, **8**, 536–542.
8 Z. Wang, T. Kadohira, T. Tada and S. Watanabe, *Nano Lett.*, 2007, **7**, 2688–2692.
9 S. H. Jo and W. Lu, *Nano Lett.*, 2008, **8**, 392–397.
10 M. Aono and T. Hasegawa, *IEEE Proc.*, 2010, **898**, 2228–2236.
11 E. Linn, R. Rosezin, C. Kugeler and R. Waser, *Nat. Mater.*, 2010, **9**, 403–406.
12 Y. V. Pershin and M. Di Ventra, *Adv. Phys.*, 2011, **60**, 145–227.
13 I. Valov, R. Waser, J. R. Jameson and M. N. Kozicki, *Nanotechnology*, 2011, **22**, 254003.
14 A. C. Torrezan, J. P. Strachan, G. Medeiros-Ribeiro and R. S. Williams, *Nanotechnology*, 2011, **22**, 485203.

15 T. Hasegawa, K. Terabe, T. Tsuruoka and M. Aono, *Adv. Mater.*, 2012, **24**, 252–267.
16 A. Chung, J. Deen, J.-S. Lee and M. Meyyappan, *Nanotechnology*, 2010, **21**, 412001.
17 L. Chua, *IEEE Trans. Circuit Theory*, 1971, **18**, 507–519.
18 T. Chang, S.-H. Jo and W. Lu, *ACS Nano*, 2011, **5**, 7669–7676.
19 T. Ohno, T. Hasegawa, T. Tsuruoka, K. Terabe, J. K. Gimzewski and M. Aono, *Nat. Mater.*, 2011, **10**, 591–595.
20 J. J. T. Wagenaar, M. Morales-Masis and J. M. van Ruitenbeek, *J. Appl. Phys.*, 2012, **111**, 014302.
21 D. B. Strukov and R. S. Williams, *Appl. Phys. A*, 2008, **94**, 515–519.
22 Z. Xu, Y. Bando, W. Wang, X. Bai and D. Golberg, *ACS Nano*, 2010, **4**, 2515–2522.
23 A. Nayak, T. Tamura, T. Tsuruoka, K. Terabe, S. Hosaka, T. Hasegawa and M. Aono, *J. Phys. Chem. Lett.*, 2010, **1**, 604–608.
24 M. Morales-Masis, S. J. van der Molen, W. T. Fu, M. B. Hesselberth and J. M. van Ruitenbeek, *Nanotechnology*, 2009, **20**, 095710.
25 M. Morales-Masis, H.-D. Wiemhöfer and J. M. van Ruitenbeek, *Nanoscale*, 2010, **2**, 2275–2280.
26 M. Morales-Masis, S. J. van der Molen, T. Hasegawa and J. M. van Ruitenbeek, *Phys. Rev. B: Condens. Matter*, 2011, **84**, 115310.
27 A. Nayak, T. Tsuruoka, K. Terabe, T. Hasegawa and M. Aono, *Appl. Phys. Lett.*, 2011, **98**, 233501.
28 S. Menzel, U. Böttger and R. Waser, *J. Appl. Phys.*, 2012, **111**, 014501.
29 I. Valov, I. Sapezanskaia, A. Nayak, T. Tsuruoka, T. Bredow, T. Hasegawa, G. Staikov, M. Aono and R. Waser, *Nat. Mater.*, 2012, **11**, 530–535.
30 I. Valov and G. Staikov, *J. Solid State Electrochem.*, 2012, **17**, 365–371.
31 Y. Yang, P. Gao, S. Gaba, T. Chang, X. Pan and W. Lu, *Nat. Commun.*, 2012, **3**, 732.
32 Q. Liu, J. Sun, H. Lv, S. Long, K. Yin, N. Wan, Y. Li, L. Sun and M. Liu, *Adv. Mater.*, 2012, **24**, 1844–1849.
33 S. Menzel, S. Tappertzhofen, R. Waser and I. Valov, *Phys. Chem. Chem. Phys.*, 2013, **15**, 6945–6952.
34 Y. Yang and W. Lu, *Nanoscale*, 2013, **5**, 10076–10092.
35 Y. Yang, P. Gao, L. Li, X. Pan, S. Tappertzhofen, S. Choi, R. Waser, I. Valov and W. D. Lu, *Nat. Commun.*, 2014, **5**, 4232.
36 F. Nardi, S. Larentis, S. Balatti, D. C. Gilmer and D. Ielmini, *IEEE Trans. Electron Devices*, 2012, **59**, 2461–2467.
37 S. Larentis, F. Nardi, S. Balatti, D. C. Gilmer and D. Ielmini, *IEEE Trans. Electron Devices*, 2012, **59**, 2468–2475.
38 P. R. Mickel, A. J. Lohn, C. D. James and M. J. Marinella, *Adv. Mater.*, 2014, **26**, 4486–4490.
39 A. Geresdi, M. Csontos, A. Gubicza, A. Halbritter and G. Mihály, *Nanoscale*, 2014, **6**, 2613.
40 A. Gubicza, M. Csontos, A. Halbritter and G. Mihály, *Nanoscale*, 2015, **7**, 4394–4399.
41 A. Geresdi, A. Halbritter, E. Szilágyi and G. Mihály, *MRS Proc.*, 2011, 1331.
42 A. Halbritter, S. Csonka, G. M. O. Y. Kolesnychenko, O. I. Shklyarevskii and H. van Kempen, *Phys. Rev. B: Condens. Matter*, 2002, **65**, 045413.
43 Y. G. Naidyuk and I. K. Yanson, *Point-Contact Spectroscopy*, Springer Verlag, Berlin, 2005.
44 B. I. Verkin, I. K. Yanson, I. O. Kulik, O. I. Shklyarevskii, A. A. Lysykh and Y. G. Naydyuk, *Solid State Commun.*, 1979, **30**, 215.
45 R. C. Emmons, C. H. Stockwell and R. H. B. Jones, *Am. Mineral.*, 1926, **11**, 326–328.
46 A. Halbritter, L. Borda and A. Zawadowski, *Adv. Phys.*, 2004, **53**, 939–1010.
47 A. Wexler, *Proc. Phys. Soc.*, 1966, **89**, 927.
48 J. Zemek, P. Jiricek, S. Hucek, A. Jablonski and B. Lesiak, *Surf. Sci.*, 2001, **473**, 8–16.
49 R. Holm, *Electric contacts*, Springer Verlag, Berlin, 1967.

